Induced correlations and rupture of molecular chaos by anisotropic dissipative Janus hard disks

Antonio Lasanta,[1,2,3,*] Aurora Torrente,[1] and Mariano López de Haro[2]

[1]*Gregorio Millán Institute of Fluid Dynamics, Nanoscience and Industrial Mathematics, Department of Materials Science and Engineering and Chemical Engineering, Universidad Carlos III de Madrid, 28911 Leganés, Spain*

[2]*Instituto de Energías Renovables, Universidad Nacional Autónoma de México (U.N.A.M.), Temixco, Morelos 62580, México*

[3]*Departamento de Álgebra. Facultad de Educación, Economía y Tecnología de Ceuta, Universidad de Granada, Cortadura del Valle, s/n. E-51001 Ceuta, Spain*

(Received 23 May 2019; published 21 November 2019)

A system of smooth "frozen" Janus-type disks is studied. Such disks cannot rotate and are divided by their diameter into two sides of different inelasticities. Taking as a reference a system of colored elastic disks, we find differences in the behavior of the collisions once the anisotropy is included. A homogeneous state, akin to the homogeneous cooling state of granular gases, is seen to arise and the singular behavior of both the collisions and the precollisional correlations are highlighted.

DOI: 10.1103/PhysRevE.100.052128

I. INTRODUCTION

Janus particles are characterized by presenting two or more different properties on their surfaces. Due to the fact that such properties allow them to have different composition and functionality [1], Janus particles offer a variety of potential applications such as drug design, biomarkers, bactericides and many others [2]. During the past few years, theoretical and experimental studies on Janus particles, as well as on their synthesis, have represented a major challenge for the scientific community (see, for instance, Refs. [3–8]). Most studies have focused their attention on equilibrium systems and the study of their phase behavior [9]. On the other hand, from a nonequilibrium perspective, only colloidal particles interacting in a solvent have been considered, thus accounting for hydrodynamic interactions but neglecting the particles' inertia [3,5–8].

It is interesting to point out that, with the proper adjustment of the parameters, a system of Janus particles embodies analogies with the so-called microswimmers, which are the prototype systems of active matter [9,10]. These swimmers, which constitute presently a "hot" and highly attractive research topic within statistical physics, are capable of self-propelling without any external energy input. Janus particles may also be employed to investigate melting and appearance of nematic phases in disks with simple inhomogeneous properties as is the case of the discotic liquid crystals [11]. The previous background serves as a motivation for the present study. Our aim is to consider a dilute or moderately dilute fluid of two-dimensional (2D) Janus particles (disks) in which these collide obeying a collision rule that reflects their asymmetry, namely, a rule in which nonhomogeneous restitution coefficients are incorporated.

Among the tools that are available to study the physical properties of fluid systems, computational simulation techniques occupy a prominent place [12,13]. Perhaps one of the most popular ones is molecular dynamics (MD) and, in the case of the less dense systems, Monte Carlo (MC) simulations of either the corresponding Boltzmann or Enskog equation. Such techniques have proven to be useful not only in the analysis of a variety of transport problems in classical fluids [12–14] but also in the successful description of the behavior of complex fluid systems and granular media [12,15–21]. In the context of this paper, a granular medium should be understood as a system composed of a huge number of particles of mesoscopic size that have mutual inelastic collisions. That is, the particles lose kinetic energy when they collide [22,23]. This loss of kinetic energy is in turn absorbed by the internal degrees of freedom of the particles of the material medium, such degrees of freedom being totally uncoupled to the dynamics of the mesoscopic particles. Given the intrinsic characteristics of these systems, a convenient way to study their physical behavior is through MD simulations, in which the (event-driven) algorithms [24] are adjusted to account for the fact that the collisions are inelastic. With such an approach, it has been possible to correctly describe laminar flow problems, instabilities, phase transitions, statistical correlations, diffusion, segregation, and other phenomena occurring in granular media [21–23,25]. Furthermore, in the case of low and moderate densities, a number of papers have demonstrated that the single-particle time-dependent velocity distribution function obeys either the Boltzmann or Enskog kinetic equations [22]. The fundamental ingredient behind both equations is the stosszahlansatz or molecular chaos assumption. It should be stressed that kinetic theory has proven to be a very accurate and powerful tool to investigate dilute granular gases made of isotropic particles [26,27]. Moreover, the use of the direct MC simulation (DSMC) method has also been successfully applied in the case of granular media [22,23,28,29]. In fact, two of us have contributed [25,30,31] to the simulation, using either MD or DSMC, of some transport problems in dilute granular gases, including the segregation of granular intruders immersed in a granular gas of rough spheres [25], a system which has received substantial recent attention in the literature [32–34]. The aim of this paper is to

*Corresponding author: alasanta@ugr.es

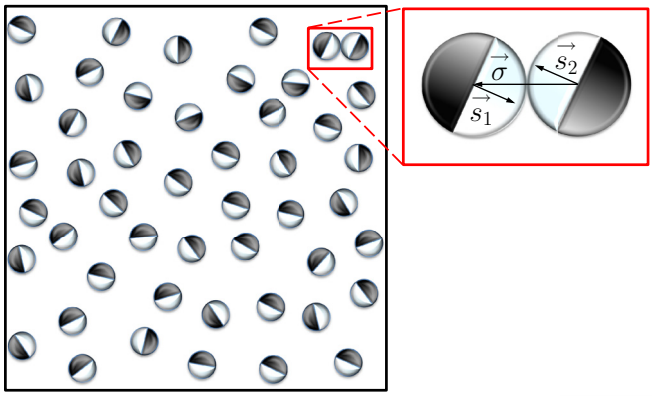

FIG. 1. Schematic representation of the collision between two Janus particles in a dilute fluid; different halves are color coded as "black" and "white." Vectors $\mathbf{s}_1$ and $\mathbf{s}_2$ are perpendicular to the diameter defining both sides.

profit from the analogies between granular media and media composed by anisotropic Janus-like particles and the computational techniques that have been employed to describe the physical properties of the former to study a dilute gas of Janus-like granular disks.

The paper is organized as follows. In order to have a proper perspective, in Sec. II we provide a brief description of the main results stemming out of the kinetic theory of a dilute gas of inelastic isotropic granular disks, including the so-called homogeneous cooling state (HCS). In Sec. III we characterize

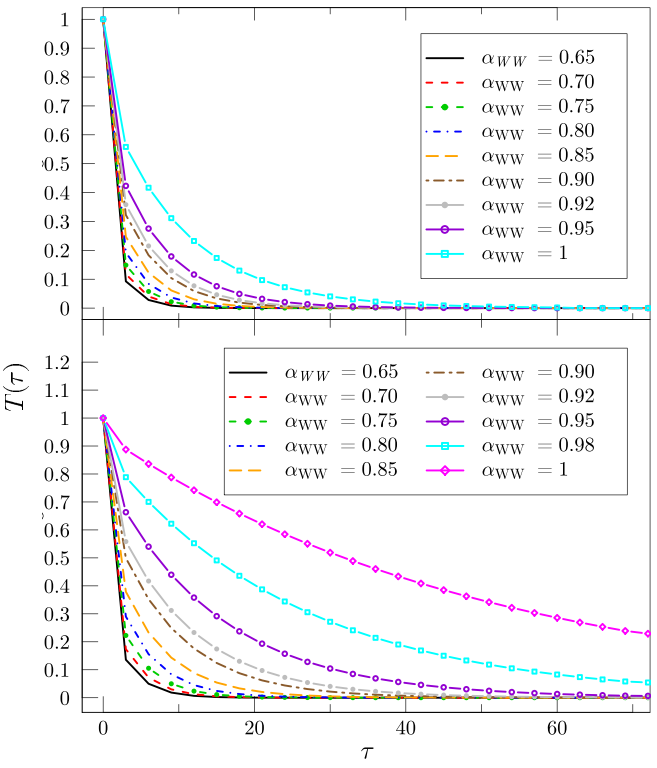

FIG. 2. Temperature vs. number of collisions per particle, τ, for $\alpha_{BB} = 0.9$ (top) and $\alpha_{BB} = 0.98$ (bottom) for different values of α_{WW} in the interval [0.65, 1.0].

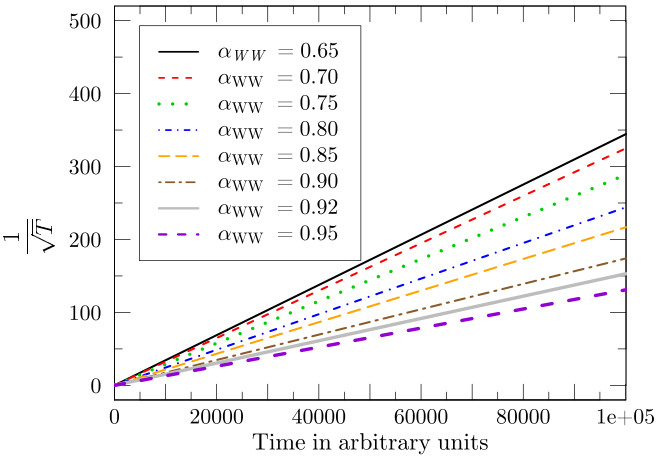

FIG. 3. Haff's law for systems with $\alpha_{BB} = 0.9$ and different values of α_{WW}. The slopes of the straight lines decrease as α_{WW} increases.

our system and the collision rule for Janus-like granular disks, where we consider varying values of the coefficients of restitution corresponding to both sides of the 2D particles and, in Sec. IV, we report our findings from numerical experiments, involving velocity distribution functions, energy time evolution, cooling rates and kurtosis. We close the paper in Sec. V with some concluding remarks.

II. THE HOMOGENEOUS COOLING STATE OF A DILUTE GAS OF ISOTROPIC GRANULAR DISKS

We begin by considering a system of N smooth inelastic hard disks, of mass $m = 1$ and diameter $\sigma = 1$. The interaction between disks is characterized by the rule:

$$\mathbf{v}_i^* = \mathbf{v}_i - \frac{1+\alpha}{2}(\mathbf{g}\cdot\widehat{\boldsymbol{\sigma}})\widehat{\boldsymbol{\sigma}},$$
$$\mathbf{v}_j^* = \mathbf{v}_j + \frac{1+\alpha}{2}(\mathbf{g}\cdot\widehat{\boldsymbol{\sigma}})\widehat{\boldsymbol{\sigma}}, \qquad (1)$$

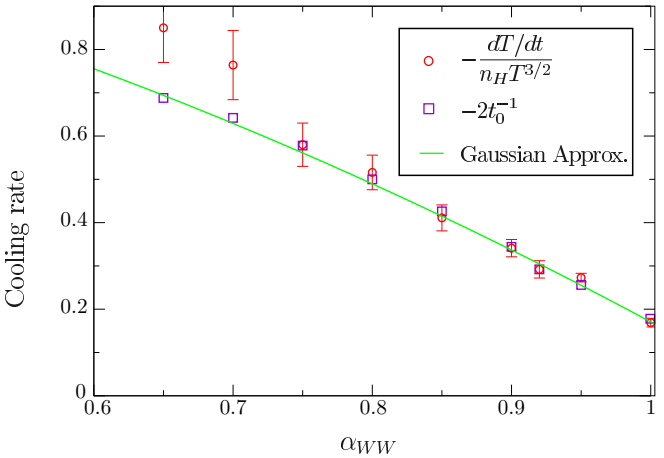

FIG. 4. Values of the total cooling rates for $\alpha_{BB} = 0.9$ and $0.65 \leqslant \alpha_{WW} \leqslant 1.0$ (open red circles), along with their confidence limits, compared with the Gaussian approximation (continuous line) as well as with the slopes of the straight lines in Fig. 3 (open magenta squares).

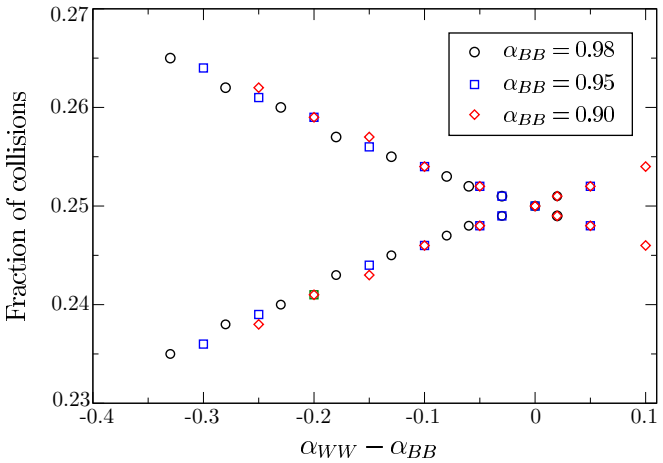

FIG. 5. Values of the fraction of collisions of each type vs. the difference $\alpha_{WW} - \alpha_{BB}$. Note the collapse into a single curve for varying values of α_{BB}. The curve with positive slope corresponds to that of *BB* type.

where we have introduced the constant coefficient of normal restitution α, the asterisks denoting velocities after the collision, $\mathbf{g} = \mathbf{v}_i - \mathbf{v}_j$ being the relative velocity, and $\widehat{\boldsymbol{\sigma}}$ a unit vector joining the centers of particles i and j at contact.

The appearance of the restitution coefficient α accounts for the loss of energy of particles i, j after the collision. Note that $\alpha \leqslant 1$, and that the value $\alpha = 1$ would correspond to elastic collisions.

The equation that properly describes this system is the Boltzmann equation of a system of freely evolving hard disks, which reads [35,36]

$$\left(\frac{\partial}{\partial t} + \mathbf{v}\cdot\nabla\right) f(\mathbf{r},\mathbf{v},t) = \mathcal{C}_B[\mathbf{r},\mathbf{v}|f(\mathbf{r},\mathbf{v},t)], \tag{2}$$

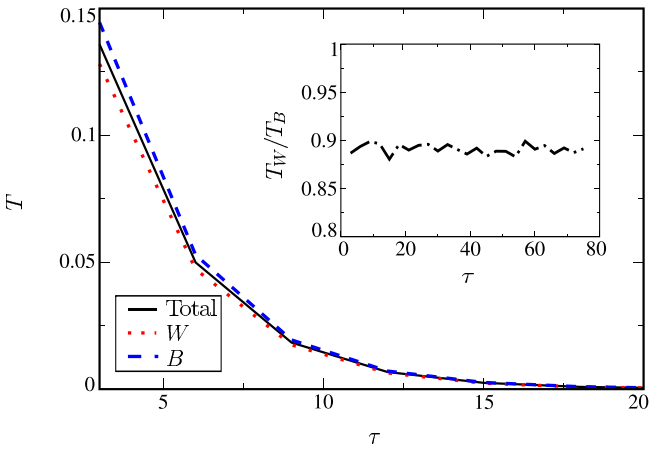

FIG. 6. Values of the temperatures of each type vs the number of collisions per particle and in a range of these between 0 and 20 for an easy visualization of the difference for $\alpha_{WW} = 0.65$ and $\alpha_{BB} = 0.98$. Note the appearance of three "temperatures" in this case. In the inset, the corresponding value of the ratio T_W/T_B between the temperatures of each kind as a function of the number of collisions per particle is shown. As pointed out in the text, this value is a constant.

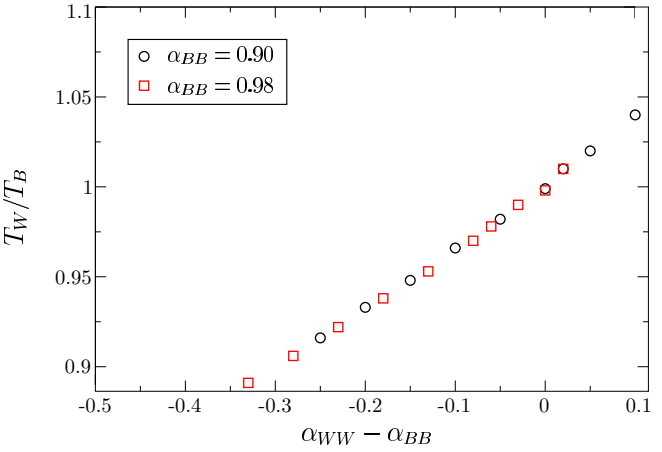

FIG. 7. Value of the ratio between the temperatures of each kind as a function of the difference $\alpha_{WW} - \alpha_{BB}$. Note again the collapse of the curves.

with $f(\mathbf{r},\mathbf{v},t)$ denoting the single-disk velocity distribution function and $\mathcal{C}_B$ the inelastic Boltzmann collision operator, namely

$$\begin{aligned}\mathcal{C}_B[\mathbf{r},\mathbf{v}|f(\mathbf{r},\mathbf{v},t)] &= \int d\mathbf{v}_1 \int d\widehat{\boldsymbol{\sigma}}\,\theta(\mathbf{g}\cdot\widehat{\boldsymbol{\sigma}})(\mathbf{g}\cdot\widehat{\boldsymbol{\sigma}}) \\ &\quad\times(\alpha^{-2}b^{-1} - 1) f(\mathbf{r},\mathbf{v},t) f(\mathbf{r},\mathbf{v}_1,t),\end{aligned} \tag{3}$$

θ is the Heaviside step function and b^{-1} an operator transforming velocities $\mathbf{v}$ and $\mathbf{v}_1$ to its right into their precollisional values. As it occurs in the purely elastic case, the derivation of this equation is based on the molecular chaos hypothesis. This means that the two-disks distribution function may be factorized in the precollisional disks as $f^{(2)}(\mathbf{x}_1,\mathbf{x}_2,t) = f(\mathbf{x}_1,t) f(\mathbf{x}_2,t)$, where $\mathbf{x}_i \equiv \{\mathbf{r}_i,\mathbf{v}_i\}$.

It is well known that when a system of inelastic particles such as the one described above is allowed to evolve freely, it reaches a homogeneous state with no fluxes or gradients, namely, the homogeneous cooling state. Such state is characterized by a single macroscopic variable, specifically the temperature $T(t)$, defined as proportional to the average kinetic energy. This variable evolves according to the so-called Haff's law [37],

$$T(t) = \frac{T(0)}{\left(1 + \dfrac{t}{t_0}\right)^2}, \tag{4}$$

where t_0 is the time characterizing the energy decay.

In the HCS, the Boltzmann equation admits a solution $f(\mathbf{v},t)$ that obeys the scaling law [35,36,38]

$$f(\mathbf{v},t) = \frac{n_H}{v_0(t)^2}\,\varpi\left[\frac{\mathbf{v}}{v_0(t)}\right], \tag{5}$$

where n_H is the homogeneous density and $v_0 = \sqrt{2k_BT}$ is the thermal velocity of the system, k_B being the Boltzmann constant. Note that for the time evolution of the system, the relevant hydrodynamic field is the temperature, which corresponds to the second moment of the velocity, namely

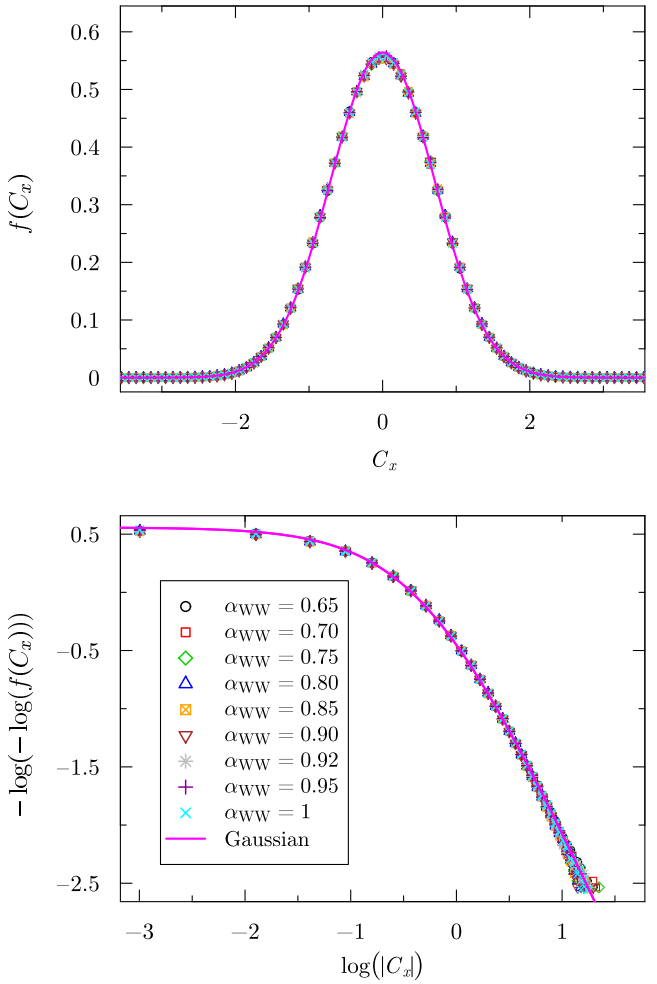

FIG. 8. Distribution function f of the x component of the velocity, C_x (top), and the $-\log\{-\log[f(C_x)]\}$ vs. $\log(|C_x|)$ (bottom) for $\alpha_{BB} = 0.9$ and $0.65 \leqslant \alpha_{WW} \leqslant 1.0$. The magenta solid line is the Maxwell-Boltzmann distribution. The linear region in the bottom panel has a slope of -1.7668, as provided by least squares.

$\langle v^2 \rangle$. On the other hand the function ϖ, which follows from the Boltzmann equation, is given by

$$\varpi(\mathbf{c}) = \pi e^{-c^2} \sum_{j \geqslant 0} a_j S^{(j)}(c^2), \quad \mathbf{c} = \frac{\mathbf{v}}{v_0}, \tag{6}$$

where $S^{(j)}$ are the Sonine polynomials, whose expressions can be found in Ref. [38].

In our case, the relevant coefficient is a_2, which is related to the kurtosis of the velocity distribution function and is given by [36,39]

$$a_2 = \tfrac{1}{2}[\langle c^4 \rangle - 2]. \tag{7}$$

It should be stressed that a_2 is very small, which means that the function ϖ is very close to the Gaussian distribution [35]. The non-Gaussianity is reflected in the exponential tails.

The expression for t_0 may be obtained from the Boltzmann equation [40], and reads:

$$t_0^{-1} \simeq \tfrac{1}{2}(1-\alpha^2)[k_B \pi T(0)]^{1/2} n_H. \tag{8}$$

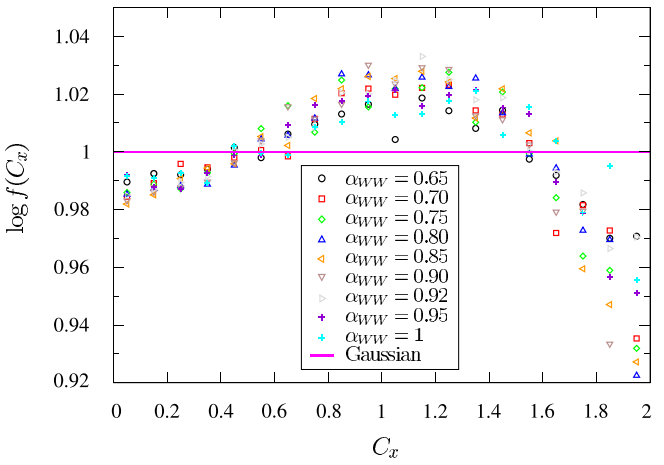

FIG. 9. Tails of the velocity distribution functions divided by the Gaussian distribution for $\alpha_{BB} = 0.9$ and $0.65 \leqslant \alpha_{WW} \leqslant 1.0$.

To close this section, and for later purposes, it is convenient to express Haff's law in terms of the average number of collisions per particle, τ, that is,

$$T(\tau) = T(0) e^{-(1-\alpha^2)\tau}, \tag{9}$$

which, interestingly, states that the kinetic energy decays exponentially with the number of collisions.

III. THE ANISOTROPIC JANUS-LIKE DISKS CASE

Let us consider now a set of N smooth anisotropic disks. Each disk comprises two parts of equal size on each side of its diameter, which are characterized by a value of the coefficient of restitution. Such values may be the same or different for both sides and either equal to one, less than one or greater than one. The disks may collide with one another in three different forms depending on which side of each disk takes part in the collision. A schematic representation of the collision is depicted in Fig. 1 and the applicable collision rule is the following:

$$\mathbf{v}_1' = \mathbf{v}_1 + \frac{1+\alpha_1(\mathbf{s}_1,\mathbf{s}_2)}{2} \widehat{\boldsymbol{\sigma}}(\mathbf{g}\cdot\widehat{\boldsymbol{\sigma}}),$$

$$\mathbf{v}_2' = \mathbf{v}_2 + \frac{1+\alpha_2(\mathbf{s}_1,\mathbf{s}_2)}{2} \widehat{\boldsymbol{\sigma}}(\mathbf{g}\cdot\widehat{\boldsymbol{\sigma}}). \tag{10}$$

Here $\mathbf{v}_i'$ indicates postcollisional velocities, $\mathbf{g} = \mathbf{v}_1 - \mathbf{v}_2$, $\widehat{\boldsymbol{\sigma}} = \frac{\mathbf{r}_1 - \mathbf{r}_2}{|\mathbf{r}_1 - \mathbf{r}_2|}$, and $\alpha_1(\mathbf{s}_1,\mathbf{s}_2)$ and $\alpha_2(\mathbf{s}_1,\mathbf{s}_2)$ are the coefficients of restitution which, as stated above, depend on the orientation of the particles at the time of the collision as given by the vectors $\mathbf{s}_1$ and $\mathbf{s}_2$. Such vectors are assigned to each of the N particles in a direction randomly distributed and perpendicular to the diameter delimiting the two (different) sides.

The dependence on $\alpha_i(\mathbf{s}_1,\mathbf{s}_2)$ may be parameterized by labeling with colors, W and B, the "white" and "black" sides, respectively, as follows:

$$\mathbf{s}_1 \cdot \widehat{\boldsymbol{\sigma}} \geqslant 0 \rightarrow \text{disk 1 side } W, \tag{11}$$

$$\mathbf{s}_1 \cdot \widehat{\boldsymbol{\sigma}} < 0 \rightarrow \text{disk 1 side } B, \tag{12}$$

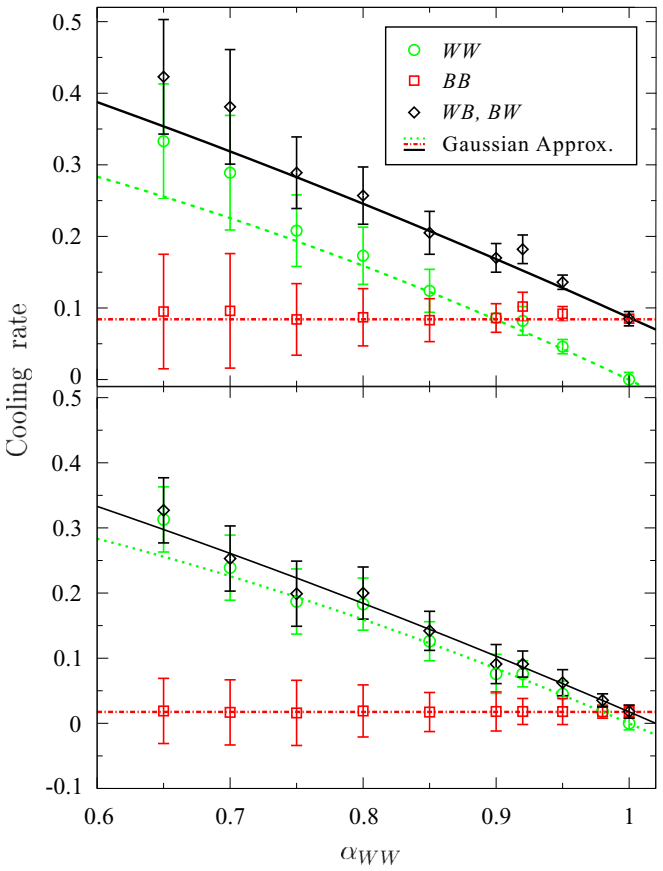

FIG. 10. Values of the cooling rates considering the collisions of types WW, BB, and two color, for $\alpha_{BB} = 0.9$ (top) and $\alpha_{BB} = 0.98$ (bottom) and for $0.65 \leqslant \alpha_{WW} \leqslant 1.0$; the straight lines correspond to the Gaussian approximation for equal fractions of collisions. Curves for BB collisions are flat since α_{BB} is kept fixed in the simulations.

$$\mathbf{s}_2 \cdot \widehat{\boldsymbol{\sigma}} < 0 \rightarrow \text{disk 2 side } W, \tag{13}$$

$$\mathbf{s}_2 \cdot \widehat{\boldsymbol{\sigma}} \geqslant 0 \rightarrow \text{disk 2 side } B, \tag{14}$$

An "event-driven" molecular dynamics algorithm has been developed to analyze the time evolution of such a system. We have taken a square box with N disks, whose diameter is σ, and a given number density ρ, which determines the size of the box. We have considered $N = k^2$ for some $k \in \mathbb{N}$ and divided the box into N square cells, so that there is one cell for each disk. Initially, the disks are centrally placed in the cells and are assigned a random velocity that follows a Maxwell-Boltzmann distribution; then they are made to elastically collide with each other until an equilibrium state is reached. After such a transient period, an anisotropy vector $\mathbf{s}_i$, whose direction is distributed uniformly in the interval $[0, 2\pi)$, is assigned to each disk. Once this has been done, the disks start to collide following the collision rules (10). Of course, the coefficients of restitution α_{BB}, α_{WW}, α_{BW}, and α_{WB}, where the subindices state the sides at contact during the collision, may be freely chosen. In particular, we have defined $\alpha_{WB} = \alpha_{BW} = \frac{\alpha_{BB}+\alpha_{WW}}{2}$.

The outcome of our simulations comprises the measurement of the velocity distribution functions for the particles, the time evolution of the energy and the kurtosis. Furthermore, we are also able to evaluate the fraction of each type of collision (and hence measure the precollisional correlations), the time evolution of the different temperatures present in the system and the cooling rates for each type of collision.

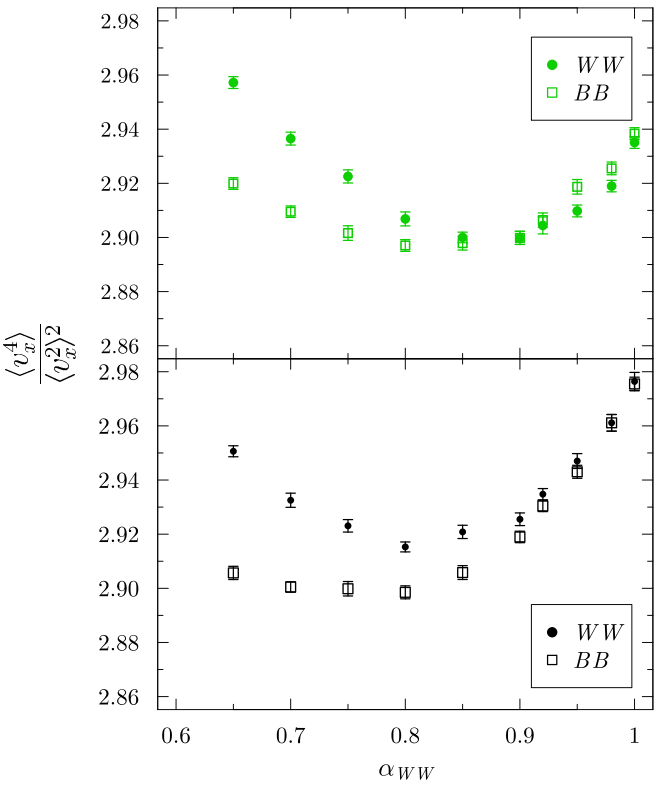

FIG. 11. Kurtosis of the velocity distribution for the collision types WW (solid circles) and BB (open squares). These values have been measured for $\alpha_{BB} = 0.90$ (top panel) and $\alpha_{BB} = 0.98$ (bottom panel), whereas α_{WW} ranges from 0.65 to 1.

IV. RESULTS

For the sake of having some reference values for later comparison with the collisional dynamics of our system of interest, and since, to the best of our knowledge, there are no previous studies in the literature of elastic colored disks, we begin with the fully elastic case. In this instance we have considered a system of 1225 disks with a number density of 0.01 and taken an average over 180 trajectories. We have taken systems with a fixed value of the coefficient of restitution α_{BB} (namely, $\alpha_{BB} = 0.9$ and $\alpha_{BB} = 0.98$) and for such systems then we have varied the value of α_{WW} in the range [0.65, 1.0]. In Fig. 2 we display the time evolution of the system temperature, time being measured as collisions per particle. In this figure, averages over the particles and trajectories have been performed. The system obeys Haff's law, as seen from the exponential decay.

This fact is more evident in Fig. 3, where straight lines of the form $T(t) = T(0)(1 + \frac{t}{t_0})^{-2}$ are obtained for $\alpha_{BB} = 0.90$ and different values of α_{WW}. In Fig. 4 we present the values of t_0^{-1} derived from the fit of the lines in Fig. 3 together with the cooling rates that have been measured directly and the

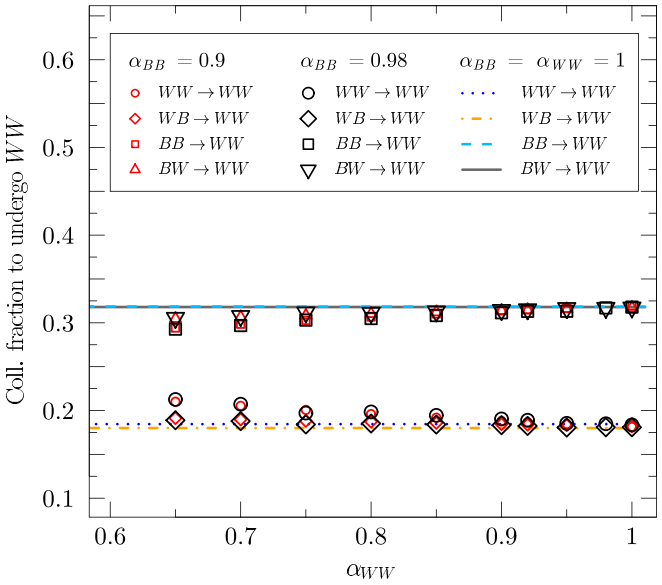

FIG. 12. Values of the conditional probabilities for the particles that, having experienced a collision of a given type (WW, WB, BB, or BW) will later undergo a WW collision. Here the coefficients of restitutions are $\alpha_{BB} = 0.9$ and 0.98, whereas $0.65 \leqslant \alpha_{WW} \leqslant 1.0$. The lines are drawn as a benchmark at the heights provided by the simulation of the completely elastic system, i.e., for $\alpha_{WW} = \alpha_{BB} = 1$.

Gaussian approximation for the value of t_0^{-1}. As it can be seen, there is an excellent agreement between the observed cooling rates for $\alpha_{WW} > 0.7$ and the value $-2/t_0$ derived from Haff's law.

A remarkable feature present in our system is the fact that, when it comes to collisions of sides of the same color, there are more collisions of one color than of the other. In order to quantify this effect, we have measured the fraction of each type of single-color collision with respect to the total number of collisions that occur in the system all along its evolution. We find that the more inelastic one color is the more collisions of this type take place. Further, this number depends only on the difference between the elasticities of the sides, as observed in Fig. 5. This leads us to suggest that different temperatures of the disks in our system may arise depending on the color of their previous collision. Also, one can see that once a disk has undergone a collision with one of its colored sides, the probability that it will collide with the opposite side (different color) is greater than the one that it will do it with the same side. This is due to the fact that such probability of collision is proportional to the relative velocities and these vectors are directed with more probability to the side opposite to the one the collision took place with.

If we measure time by collisions per particle, at any temporal point we can consider the particles that have collided either with one side (color) or with the other and investigate two additional "temperatures," T_W and T_B, each one corresponding to one color. In Fig. 6 it can be immediately seen that the particles that have collided with the black side have a greater temperature than those that have collided with the white side. This is not surprising since the white side has a coefficient of restitution $\alpha_W < \alpha_B$. On the other hand, we also find that the ratio between both temperatures T_W and T_B is a constant (cf. inset in Fig. 6) and that it depends only on the difference $\alpha_{WW} - \alpha_{BB}$ (cf. Fig. 7).

This phenomenon can be related to that occurring in binary mixtures of hard isotropic grains that are either freely cooling [41] or subject to a vibration [42,43]. In these situations, a breakdown of energy equipartition has been observed, with species involved in the experiments exhibiting different partial temperatures but equal cooling rates. However, in our system the two distinct temperatures are observed in two collections of (anisotropic) particles with identical material properties but having undergone different previous collisions.

The velocity distribution functions corresponding to $\alpha_{BB} = 0.9$ for the x component of the scaled velocity, C_x, are shown in Fig. 8. To a good approximation, they may be taken as Gaussian distributions. Also, the tails of the scaled distributions are displayed in Fig. 9. All these curves are similar to the ones obtained in isotropic granular media [35,36,44].

We further analyzed the cooling rates corresponding to the different types of collisions: single color (WW and BB) or two color (either WB or BW). These have been measured directly from the dissipated energy at given time intervals for $\alpha_{BB} = 0.9$ and $\alpha_{BB} = 0.98$ and varying α_{WW} between 0.65 and 1.0. The results are displayed in Fig. 10; note that the top panel of this figure corresponds to the data reported in Fig. 4. At the values where $\alpha_{BB} = \alpha_{WW}$ the cooling rate for the two-color case is exactly two times that of the single-color one (i.e., WW or BB), as it is accounting for two types of collisions (WB and BW).

We have also measured the kurtosis of the collisions of types BB and WW for the same collection of values of the parameters α_{WW} and α_{BB} as in Fig. 10. We observe that distinct coefficients of restitution lead to different kurtosis, as shown in Fig. 11, and that these outcomes are also close to the Gaussian distribution. Again, the results in Figs. 10 and 11 are found to be qualitatively similar to those reported in Refs. [35,36].

Once the existence of a difference between the fraction of collisions of each type, the cooling rates and the temperatures has been noticed, the next natural step is to consider the precollisional correlations. The idea behind this analysis is to investigate whether the consideration of anisotropic disks may produce an effect on the dynamics of the collisions.

We have measured the precollisional correlations for the four kinds of collision and taken as the reference system the one of colored but elastic disks. To that end, a numeric label, 1, 2, 3, or 4, is assigned to each disk after it collides, to account for the sides at contact. This label is checked against the value it had prior to collision, where we had made a distinction between the four possible types. We have found that there seems not to be a big effect as the values of the inelasticities are varied in the interval [0.65, 1]. In fact, there is only a small precollisional correlation of the colliding colors related to them, as shown in Fig. 12. In this figure, we have represented the conditional probabilities of having a WW collision provided that the previous collision was of one of the four alternatives.

It is clear that, as α_{WW} increases, these conditional probabilities tend to approach the values corresponding to the completely elastic system, represented as straight lines in

Fig. 12. The two distinct possible probabilities for each system observed in this plot correspond to the situations of a disk colliding with the same side as the one involved in the previous collision (low values) or with the opposite side (high values).

However, when α_{WW} decreases toward 0, the probabilities of undergoing a WW-type collision after one of type BB and of type BW tend to progressively differ. The same effect is observed for the conditional probabilities given that a WW or WB collision has occurred. Moreover, when α_{WW} approaches 0, the probabilities of a WW collision after one of type BB and WW are close to 0.22 and 0.30, respectively.

Similar results are obtained for the other combinations, as reported in Tables I–III of the Appendix, where each entry in the "C.Prob." columns provides the conditional probability as the fraction of the corresponding collisions (for instance, when the collision is of the type WW (1) and previously it has been of the type WW (1), WB (2), BB (3), or BW (4), and similarly for all suitable combinations).

V. CONCLUDING REMARKS

In this paper we have addressed a system of inelastic Janus-like disks by means of extensive numerical experiments. In particular we have measured different statistical quantities, namely, temperature evolution, velocity distribution functions, kurtosis, and precollisional correlations. We find that for this system a HCS also arises even in the presence of correlations. In particular, a Haff's law is obeyed by the temperature irrespective of the fact that the molecular chaos assumption does not hold here. As far as we are aware, this is the first time that such a system, along with some of its features, has been reported. This opens new avenues for research including, for instance, stationary states sustained by injection of energy, rough disks, smooth or rough spheres and the analysis of problems like segregation [45,46], memory effects [30,31,47–53], and shear states [14,54]. Of particular interest are the studies of the clustering formation processes and the phase transitions that may arise as the density is increased. We plan to examine some of these problems in the near future.

ACKNOWLEDGMENTS

We are indebted to M. J. Ruiz-Montero (deceased) and J. J. Brey for suggesting this project to one of us (A.L.). This work has been partially supported by the Spanish Ministerio de Ciencia, Innovación y Universidades and the Agencia Estatal de Investigación Grants (partially financed by the ERDF) No. MTM2017-84446-C2-2-R (A.L. and A.T.) and No. FIS2017-84440-C2-2-P (A.T.). A.L. also acknowledges the Program José Castillejos, funded by the Spanish Ministerio de Ciencia, Innovación y Universidades Grant No. CAS18/00335, which allowed him to visit the Instituto de Energías Renovables (U.N.A.M.), where this work was carried out.

APPENDIX

For completeness, we assemble in this Appendix the conditional probabilities of a collision of type 1, 2, 3, or 4, provided that the preceding collision was of one of these four types, for different values of α_{BB} and α_{WW}.

TABLE I. Precollisional correlations for $\alpha_{BB} = 0.9$ and 0.98 and for $\alpha_{WW} = 0.65$, 0.7, and 0.75.

α_{BB}	α_{WW}	Type	C.Prob.	α_{BB}	α_{WW}	Type	C.Prob.
		$1 \to 1$	0.2100			$1 \to 1$	0.2126
		$2 \to 1$	0.1912			$2 \to 1$	0.1889
		$3 \to 1$	0.2941			$3 \to 1$	0.2928
		$4 \to 1$	0.3047			$4 \to 1$	0.3057
		$1 \to 2$	0.2043			$1 \to 2$	0.2062
		$2 \to 2$	0.1943			$2 \to 2$	0.1921
		$3 \to 2$	0.2957			$3 \to 2$	0.2947
		$4 \to 2$	0.3057			$4 \to 2$	0.3070
	0.65	$1 \to 3$	0.3194		0.65	$1 \to 3$	0.3244
		$2 \to 3$	0.3110			$2 \to 3$	0.3136
		$3 \to 3$	0.1800			$3 \to 3$	0.1747
		$4 \to 3$	0.1896			$4 \to 3$	0.1872
		$1 \to 4$	0.3190			$1 \to 4$	0.3235
		$2 \to 4$	0.3091			$2 \to 4$	0.3118
		$3 \to 4$	0.1774			$3 \to 4$	0.1725
		$4 \to 4$	0.1945			$4 \to 4$	0.1921
		$1 \to 1$	0.2053			$1 \to 1$	0.2072
		$2 \to 1$	0.1898			$2 \to 1$	0.1879
		$3 \to 1$	0.2984			$3 \to 1$	0.2969
		$4 \to 1$	0.3065			$4 \to 1$	0.3078
		$1 \to 2$	0.1999			$1 \to 2$	0.2013
		$2 \to 2$	0.1930			$2 \to 2$	0.1908
		$3 \to 2$	0.2999			$3 \to 2$	0.2988
		$4 \to 2$	0.3073			$4 \to 2$	0.3090
0.9	0.7	$1 \to 3$	0.3179	0.98	0.7	$1 \to 3$	0.3231
		$2 \to 3$	0.3117			$2 \to 3$	0.3144
		$3 \to 3$	0.1817			$3 \to 3$	0.1762
		$4 \to 3$	0.1887			$4 \to 3$	0.1861
		$1 \to 4$	0.3177			$1 \to 4$	0.3223
		$2 \to 4$	0.3099			$2 \to 4$	0.3127
		$3 \to 4$	0.1791			$3 \to 4$	0.1739
		$4 \to 4$	0.1932			$4 \to 4$	0.1909
		$1 \to 1$	0.2007			$1 \to 1$	0.1971
		$2 \to 1$	0.1881			$2 \to 1$	0.1841
		$3 \to 1$	0.3027			$3 \to 1$	0.3031
		$4 \to 1$	0.3084			$4 \to 1$	0.3119
		$1 \to 2$	0.1956			$1 \to 2$	0.1921
		$2 \to 2$	0.1916			$2 \to 2$	0.1872
		$3 \to 2$	0.3040			$3 \to 2$	0.3045
		$4 \to 2$	0.3088			$4 \to 2$	0.3124
	0.75	$1 \to 3$	0.3168		0.75	$1 \to 3$	0.3184
		$2 \to 3$	0.3122			$2 \to 3$	0.3134
		$3 \to 3$	0.1834			$3 \to 3$	0.1785
		$4 \to 3$	0.1875			$4 \to 3$	0.1845
		$1 \to 4$	0.3164			$1 \to 4$	0.3207
		$2 \to 4$	0.3111			$2 \to 4$	0.3149
		$3 \to 4$	0.1807			$3 \to 4$	0.1771
		$4 \to 4$	0.1919			$4 \to 4$	0.1889

TABLE II. Precollisional correlations for $\alpha_{BB} = 0.9$ and 0.98 and for $\alpha_{WW} = 0.8$, 0.85, and 0.9.

α_{BB}	α_{WW}	Type	C.Prob.	α_{BB}	α_{WW}	Type	C.Prob.
		$1 \to 1$	0.1959			$1 \to 1$	0.1984
		$2 \to 1$	0.1872			$2 \to 1$	0.1852
		$3 \to 1$	0.3066			$3 \to 1$	0.3049
		$4 \to 1$	0.3103			$4 \to 1$	0.3114
		$1 \to 2$	0.1917			$1 \to 2$	0.1933
		$2 \to 2$	0.1904			$2 \to 2$	0.1886
		$3 \to 2$	0.3072			$3 \to 2$	0.3063
		$4 \to 2$	0.3107			$4 \to 2$	0.3118
	0.8	$1 \to 3$	0.3157		0.8	$1 \to 3$	0.3205
		$2 \to 3$	0.3129			$2 \to 3$	0.3154
		$3 \to 3$	0.1850			$3 \to 3$	0.1798
		$4 \to 3$	0.1863			$4 \to 3$	0.1843
		$1 \to 4$	0.3156			$1 \to 4$	0.3202
		$2 \to 4$	0.3120			$2 \to 4$	0.3144
		$3 \to 4$	0.1818			$3 \to 4$	0.1770
		$4 \to 4$	0.1907			$4 \to 4$	0.1885
		$1 \to 1$	0.1918			$1 \to 1$	0.1945
		$2 \to 1$	0.1858			$2 \to 1$	0.1840
		$3 \to 1$	0.3101			$3 \to 1$	0.3083
		$4 \to 1$	0.3122			$4 \to 1$	0.3131
		$1 \to 2$	0.1876			$1 \to 2$	0.1898
		$2 \to 2$	0.1893			$2 \to 2$	0.1875
		$3 \to 2$	0.3106			$3 \to 2$	0.3094
		$4 \to 2$	0.3125			$4 \to 2$	0.3132
0.9	0.85	$1 \to 3$	0.3146	0.98	0.85	$1 \to 3$	0.3195
		$2 \to 3$	0.3136			$2 \to 3$	0.3160
		$3 \to 3$	0.1866			$3 \to 3$	0.1810
		$4 \to 3$	0.1851			$4 \to 3$	0.1834
		$1 \to 4$	0.3149			$1 \to 4$	0.3190
		$2 \to 4$	0.3126			$2 \to 4$	0.3153
		$3 \to 4$	0.1832			$3 \to 4$	0.1778
		$4 \to 4$	0.1894			$4 \to 4$	0.1878
		$1 \to 1$	0.1880			$1 \to 1$	0.1904
		$2 \to 1$	0.1844			$2 \to 1$	0.1833
		$3 \to 1$	0.3136			$3 \to 1$	0.3115
		$4 \to 1$	0.3139			$4 \to 1$	0.3147
		$1 \to 2$	0.1844			$1 \to 2$	0.1862
		$2 \to 2$	0.1882			$2 \to 2$	0.1863
		$3 \to 2$	0.3137			$3 \to 2$	0.3125
		$4 \to 2$	0.3136			$4 \to 2$	0.3149
	0.9	$1 \to 3$	0.3136		0.9	$1 \to 3$	0.3182
		$2 \to 3$	0.3140			$2 \to 3$	0.3168
		$3 \to 3$	0.1879			$3 \to 3$	0.1824
		$4 \to 3$	0.1846			$4 \to 3$	0.1826
		$1 \to 4$	0.3140			$1 \to 4$	0.3185
		$2 \to 4$	0.3135			$2 \to 4$	0.3156
		$3 \to 4$	0.1845			$3 \to 4$	0.1792
		$4 \to 4$	0.1880			$4 \to 4$	0.1866

TABLE III. Precollisional correlations for $\alpha_{BB} = 0.9$ and 0.98 and for $\alpha_{WW} = 0.92$, 0.95, and 1.

α_{BB}	α_{WW}	Type	C.Prob.	α_{BB}	α_{WW}	Type	C.Prob.
		$1 \to 1$	0.1866			$1 \to 1$	0.1889
		$2 \to 1$	0.1838			$2 \to 1$	0.1824
		$3 \to 1$	0.3149			$3 \to 1$	0.3131
		$4 \to 1$	0.3146			$4 \to 1$	0.3155
		$1 \to 2$	0.1829			$1 \to 2$	0.1847
		$2 \to 2$	0.1881			$2 \to 2$	0.1862
		$3 \to 2$	0.3147			$3 \to 2$	0.3135
		$4 \to 2$	0.3142			$4 \to 2$	0.3155
	0.92	$1 \to 3$	0.3130		0.92	$1 \to 3$	0.3177
		$2 \to 3$	0.3141			$2 \to 3$	0.3169
		$3 \to 3$	0.1888			$3 \to 3$	0.1832
		$4 \to 3$	0.1840			$4 \to 3$	0.1821
		$1 \to 4$	0.3134			$1 \to 4$	0.3179
		$2 \to 4$	0.3138			$2 \to 4$	0.3162
		$3 \to 4$	0.1848			$3 \to 4$	0.1797
		$4 \to 4$	0.1879			$4 \to 4$	0.1862
		$1 \to 1$	0.1845			$1 \to 1$	0.1854
		$2 \to 1$	0.1832			$2 \to 1$	0.1806
		$3 \to 1$	0.3166			$3 \to 1$	0.3132
		$4 \to 1$	0.3156			$4 \to 1$	0.3169
		$1 \to 2$	0.1811			$1 \to 2$	0.1817
		$2 \to 2$	0.1870			$2 \to 2$	0.1842
		$3 \to 2$	0.3170			$3 \to 2$	0.3136
		$4 \to 2$	0.3148			$4 \to 2$	0.3167
0.9	0.95	$1 \to 3$	0.3124	0.98	0.95	$1 \to 3$	0.3154
		$2 \to 3$	0.3145			$2 \to 3$	0.3150
		$3 \to 3$	0.1896			$3 \to 3$	0.1827
		$4 \to 3$	0.1834			$4 \to 3$	0.1819
		$1 \to 4$	0.3129			$1 \to 4$	0.3181
		$2 \to 4$	0.3141			$2 \to 4$	0.3171
		$3 \to 4$	0.1859			$3 \to 4$	0.1807
		$4 \to 4$	0.1870			$4 \to 4$	0.1858
		$1 \to 1$	0.1812			$1 \to 1$	0.1836
		$2 \to 1$	0.1819			$2 \to 1$	0.1809
		$3 \to 1$	0.3196			$3 \to 1$	0.3179
		$4 \to 1$	0.3171			$4 \to 1$	0.3175
		$1 \to 2$	0.1781			$1 \to 2$	0.1799
		$2 \to 2$	0.1862			$2 \to 2$	0.1845
		$3 \to 2$	0.3194			$3 \to 2$	0.3185
		$4 \to 2$	0.3162			$4 \to 2$	0.3171
	1	$1 \to 3$	0.3117		1	$1 \to 3$	0.3169
		$2 \to 3$	0.3149			$2 \to 3$	0.3170
		$3 \to 3$	0.1909			$3 \to 3$	0.1855
		$4 \to 3$	0.1825			$4 \to 3$	0.1806
		$1 \to 4$	0.3122			$1 \to 4$	0.3172
		$2 \to 4$	0.3150			$2 \to 4$	0.3167
		$3 \to 4$	0.1866			$3 \to 4$	0.1814
		$4 \to 4$	0.1861			$4 \to 4$	0.1846

[1] E. Poggi, J.-F. Gohy, Colloid Polym. Sci. **295**, 2083 (2017).

[2] Z. Lin and B. Li, *Soft, Hard, and Hybrid Janus Structures Synthesis, Self-Assembly, and Applications* (World Scientific, Washington, DC, 2017).

[3] P. K. Ghosh, V. R. Misko, F. Marchesoni, and F. Nori, Phys. Rev. Lett. **110**, 268301 (2013).

[4] Z. Rozynek, A. Mikkelsen, P. Dommersnes, and J. O. Fossum, Nat. Commun. **5**, 3945 (2014).

[5] S. C. Glotzer and M. J. Solomon, Nat. Mater. **6**, 557 (2014).
[6] J. Zhang, E. Luijten, and S. Granick, Ann. Rev. Phys. Chem. **66**, 581 (2015).
[7] J. R. Gómez-Solano, A. Blokhuis, and C. Bechinger, Phys. Rev. Lett. **116**, 138301 (2016).
[8] S. A. Mallory, C. Valeriani, and A. Cacciuto, Ann. Rev. Phys. Chem. **69**, 59 (2018).
[9] R. Fantoni, *The Janus Fluid* (Springer, New York, 2013).
[10] F. Alarcon, E. Navarro-Argemí, C. Valeriani, and I. Pagonabarraga, Phys. Rev. E **99**, 062602 (2019).
[11] T. Wöhrle, I. Wurzbach, J. Kirres, A. Kostidou, N. Kapernaum, J. Litterscheidt, J. C. Haenle, P. Staffeld, A. Baro, F. Giesselmann, and S. Laschat, Chem. Rev. **116**, 1139 (2015).
[12] D. C. Rapaport, *The Art of Molecular Dynamics Simulation*, 2nd ed. (Cambridge University Press, Cambridge, 2004).
[13] G. I. Bird, *Molecular Gas Dynamics and the Direct Simulation of Gas Flows* (Clarendon, Oxford, 1994).
[14] V. Garzó and A. Santos, *Kinetic Theory of Gases in Shear Flows* (Kluwer, Dordrech, 2003).
[15] T. Pöschel and T. Schwager, *Computational Granular Dynamics* (Springer, New York, 2005).
[16] A. Puglisi, *Transport and Fluctuations in Granular Fluids: From Boltzmann Equation to Hydrodynamics, Diffusion and Motor Effects* (Springer, Berlin, 2014).
[17] A. Prados, A. Lasanta, and P. I. Hurtado, Phys. Rev. Lett. **107**, 140601 (2011).
[18] A. Lasanta, A. Manacorda, A. Prados, and A. Puglisi, New J. Phys. **17**, 083039 (2015).
[19] A. Prados, A. Lasanta, and P. I. Hurtado, Phys. Rev. E **86**, 031134 (2012).
[20] A. Lasanta, P. I. Hurtado, and A. Prados, Eur. Phys. J. E **39**, 35 (2015).
[21] C. A. Plata, A. Manacorda, A. Lasanta, A. Puglisi, and A. Prados, J. Stat. Mech.: Theory Exp. (2016) 093203.
[22] I. Goldhirsch, Annu. Rev. Fluid Mech. **35**, 267 (2003).
[23] I. S. Aranson and L. S. Tsimring, Rev. Mod. Phys. **78**, 641 (2006).
[24] M. P. Allen and D. J. Tildesley, *Computer Simulation of Liquids* (Oxford Science, Oxford, 1989).
[25] F. Vega Reyes, A. Lasanta, A. Santos, and V. Garzó, Phys. Rev. E **96**, 052901 (2017).
[26] V. Garzó, *Granular Gaseous Flows* (Springer Nature Switzerland, Cham, 2019).
[27] A. Puglisi, *Transport and Fluctuations in Granular Fluids* (Springer, Berlin, 2015).
[28] J. M. Montanero and A. Santos, Gran. Matt. **2**, 53 (2000).
[29] J. M. Montanero and V. Garzó, Gran. Matt. **4**, 17 (2002).
[30] A. Lasanta, F. Vega Reyes, A. Prados, and A. Santos, Phys. Rev. Lett. **119**, 148001 (2017).
[31] A. Torrente, M. A. López-Castaño, A. Lasanta, F. V. Reyes, A. Prados, and A. Santos, Phys. Rev. E **99**, 060901(R) (2019).
[32] A. Lasanta, F. Vega Reyes, V. Garzó, and A. Santos, Phys. Fluids **31**, 063306 (2019).
[33] N. V. Brilliantov, T. Pöschel, W. T. Kranz, and A. Zippelius, Phys. Rev. Lett. **98**, 128001 (2007).
[34] F. Vega Reyes and A. Santos, Phys. Fluids **27**, 113301 (2015).
[35] J. J. Brey, M. J. Ruiz-Montero, and D. Cubero, Phys. Rev. E **54**, 3664 (1996).
[36] J. J. Brey and M. J. Ruiz-Montero, Phys. Rev. E **69**, 011305 (2004).
[37] P. K. Haff, J. Fluid Mech. **134**, 401 (1983).
[38] P. Resibois and M. De Leener, *Classical Kinetic Theory of Fluids* (John Wiley & Sons, New York, 1977).
[39] T. P. C. van Noije and M. H. Ernst, Gran. Matt. **1**, 57 (1998).
[40] J. J. Brey, J. W. Dufty, C. S. Kim, and A. Santos, Phys. Rev. E **58**, 4638 (1998).
[41] V. Garzó and J. Dufty, Phys. Rev. E **60**, 5706 (1999).
[42] R. D. Wildman and D. J. Parker, Phys. Rev. Lett. **88**, 064301 (2002).
[43] K. Feitosa and N. Menon, Phys. Rev. Lett. **88**, 198301 (2002).
[44] F. Rouyer and N. Menon, Phys. Rev. Lett. **85**, 3676 (2000).
[45] V. Garzó, J. A. Murray, and F. Vega Reyes, Phys. Fluids **25**, 043302 (2013).
[46] F. V. Reyes, V. Garzó, and N. Khalil, Phys. Rev. E **89**, 052206 (2014).
[47] A. Lasanta, F. Vega Reyes, A. Prados, and A. Santos, New J. Phys. **21**, 033042 (2019).
[48] A. Prados and E. Trizac, Phys. Rev. Lett. **112**, 198001 (2014).
[49] E. Trizac and A. Prados, Phys. Rev. E **90**, 012204 (2014).
[50] N. C. Keim, J. D. Paulsen, Z. Zeravcic, S. Sastry, and S. R. Nagel, Rev. Mod. Phys. **91**, 035002 (2019).
[51] F. V. Reyes and A. Lasanta, in *Proceedings of the 31st International Symposium on Rarefied Gas Dynamics: RGD31*, edited by Y. Zhang, D. R. Emerson, D. Lockerby, and L. Wu, AIP Conf. Proc. No. 2132 (AIP, New York, 2019), p. 080004.
[52] M. Baity-Jesi, E. Calore, A. Cruz, L. A. Fernández, J. M. Gil-Narvión *et al.*, Proc. Natl. Acad. Sci. USA **116**, 15350 (2019).
[53] A. Gijón, A. Lasanta, and E. R. Hernández, Phys. Rev. E **100**, 032103 (2019).
[54] V. Garzó, Phys. Rev. E **48**, 3589 (1993).